

Preferential Attachments of Organic Dyes onto {101} Facets of TiO₂ Nanoparticles

Feiyu Diao,[†] Wenshuang Liang,[†] Fenghui Tian,[†] Yiqian Wang,^{*,†,‡,§} Paola Vivo,^{||} Alexander Efimov,^{||} and Helge Lemmetyinen^{||}

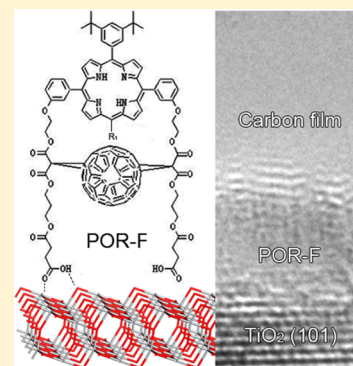
[†]The Cultivation Base for State Key Laboratory & College of Chemical Science and Engineering, Qingdao University, No. 308, Ningxia Road, Qingdao 266071, P. R. China

[‡]College of Physics, Qingdao University, No. 308, Ningxia Road, Qingdao, 266071, P. R. China

[§]Key Laboratory of Photonics Materials and Technology in University of Shandong, Qingdao University, No. 308, Ningxia Road, Qingdao 266071, P.R. China

^{||}Department of Chemistry and Bioengineering, Tampere University of Technology, P. O. Box 541, FIN-33101 Tampere, Finland

ABSTRACT: Hybrid nanostructures of organic dyes/TiO₂ nanoparticles were successfully fabricated by self-assembly method. Compared with pure organic dyes, these hybrid nanostructures showed enhanced performance of light absorption. Extensive high-resolution transmission electron microscopy observations demonstrated that the organic dyes are preferentially attached onto the {101} facets of anatase TiO₂ nanoparticles. Density functional theory calculations further confirmed that the preferential attachments are reasonable. These discoveries are very important for the preparation and improvement of the dye-sensitized and hybrid solar cells.



INTRODUCTION

The huge gap between the present use of solar energy and its unexploited potential application represents a great challenge in the energy research. As one of the most important ways to use solar energy, solar cells have gained much attention in recent years.^{1,2} Organic solar cells (OSCs) are an attractive technology in the solar energy research for their light weight, low cost, flexibility, and versatility in the fabrication schemes.^{3,4} Indeed, much work must be done to overcome the main difficulties for this technology, that is, enhancement of cell efficiency and lifetime. Thus, the need for novel materials acting as electron acceptors and donors and the understanding of the interplay between interfaces of electrodes are currently under intense investigation. Hybrid organic–inorganic nanostructures, consisting of an inorganic semiconductor coupled to an organic dye, have emerged as a key enabler for photovoltaics during the recent years due to their peculiar structures and remarkable optical, electrical, chemical, and magnetic properties that differ significantly from those of bulk materials.⁵

Since Fujishima and Honda discovered the photocatalytic splitting of water on titanium dioxide (TiO₂) electrode under ultraviolet (UV) light in 1972, TiO₂ materials have attracted considerable attention due to their great potential applications in catalysis, photocatalysis, and especially dye-sensitized solar cells (DSSC).^{6–9} TiO₂ has been applied extensively in photovoltaic devices, for example, as interfacial layers in OSC^{10,11} and as a part of the active device constituents acting

as electron transport materials in DSSC and hybrid solar cells (HSCs).^{12,13} Power conversion efficiency in organic photovoltaics (OPVs) is highly dependent on parameters such as open-circuit voltage (V_{oc}), which, in turn, is significantly affected by the interfaces between active materials (donor and acceptor).^{14–16} These studies reveal the urgent need to investigate and understand interfacial microstructures in these photovoltaic systems.

We report on the microstructure and light absorption properties of hybrid organic/TiO₂ nanoparticles fabricated by self-assembly method. We have found that the organic dyes have priority of adsorbing onto the {101} facets of anatase TiO₂ nanoparticles. These hybrid organic/TiO₂ nanostructures show the ability to promote the light absorption. Furthermore, extensive DFT calculations are performed to investigate the preferential adsorption theoretically.

EXPERIMENTAL SECTION

Preparation of TiO₂ Films. TiO₂ nanoparticles with an average diameter of 15 nm were prepared according to the literature protocol.¹⁷ TiO₂ films were deposited onto glass plates by doctor-blade technique, which is shown in Figure 1a. A precleaned glass plate (2 cm × 3.5 cm), with the edges

Received: February 10, 2015

Revised: April 2, 2015

Published: April 2, 2015

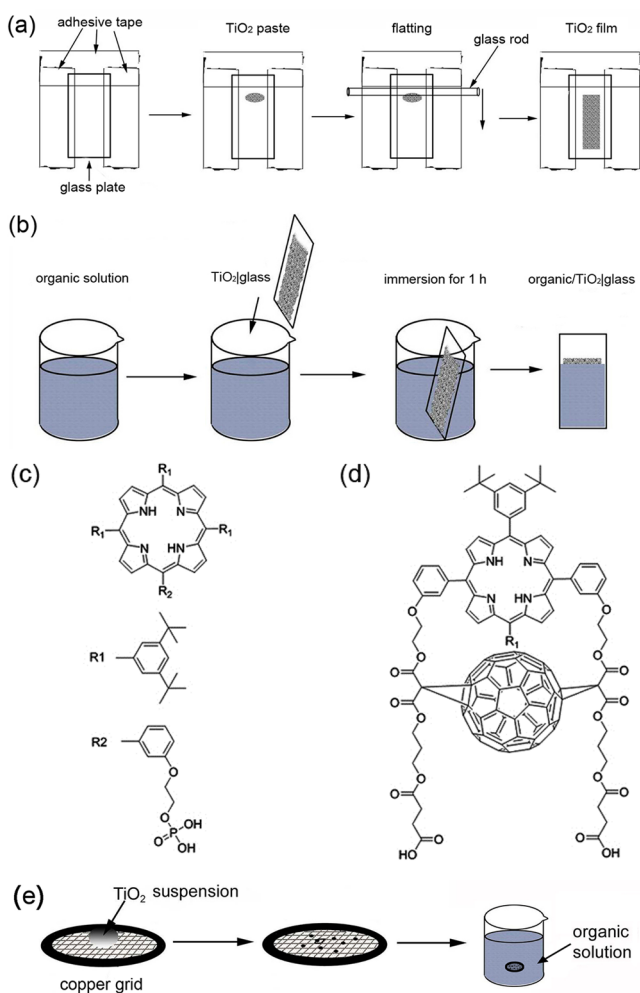


Figure 1. (a) Preparation of TiO₂ films using doctor-blade technique; (b) Preparation of hybrid organic/TiO₂ films by self-assembly method; Structures of POR-P (c) and POR-F (d); (e) TEM specimen preparation procedure of hybrid organic/TiO₂ nanostructures.

covered by adhesive tapes, was used as the substrate. One drop of TiO₂ paste was spread on the plate with a glass rod. After drying the film at 125 °C for 5 min, the samples were gradually annealed in an air flow at 325 °C for 5 min, at 375 °C for 5 min, at 450 °C for 15 min, and at 500 °C for 15 min.

Preparation and Characterization of Hybrid Organic/TiO₂ Films. Hybrid organic/TiO₂ films were fabricated by self-assembly method, as shown in Figure 1b. Figure 1c,d shows the molecular structures of two novel organic dyes, porphyrin-phosphate (POR-P) and porphyrin-fullerene (POR-F). First, the organic solutions (0.20 mM) were prepared by dissolving POR-P (or POR-F) into a mixture of ethanol and chloroform (1:1). Then TiO₂ films were immersed into the organic solution for 1 h. Subsequently, the samples were rinsed and immersed in ethanol to remove residual organic molecules.

TEM Specimen Preparation and Characterization of Hybrid Organic/TiO₂ Nanostructures. As shown in Figure 1e, TiO₂ paste was first dispersed onto a holey-carbon-film-coated copper grid. Then, the copper grid was immersed in the organic solution for 1 h. Finally, the copper grid was rinsed with ethanol to remove residual unbound organic molecules.

Bright-field (BF) transmission electron microscopy (TEM) and high-resolution TEM (HRTEM) examinations were

carried out using a JEOL JEM 2100F transmission electron microscope operating at 200 kV, whose point-to-point resolution is 2.4 Å.

Light Absorption Measurement of Hybrid Organic/TiO₂ Nanomaterials. Shimadzu UV-3600 spectrophotometer was used to measure the light absorption of these hybrid organic/TiO₂ films and of pure organic solutions, respectively. The hybrid organic/TiO₂ glasses were cut into 1 cm × 3.5 cm for the light absorption measurements. The UV-vis absorption spectra of the solutions were measured in a 1 cm cuvette.

RESULTS AND DISCUSSION

Figure 2 shows the steady-state UV absorption spectra of hybrid organic dyes/TiO₂ films and pure organic dye solutions. In Figure 2a, the absorption spectra of pure POR-F solution (black line) and the hybrid POR-F/TiO₂ films (red line) show the typical characteristic bands of the free base porphyrin, where the strongest absorption of Soret band appears at 420 nm and four weaker Q bands at 520, 550, 590, and 650 nm, respectively. Figure 2b shows the zoomed absorption spectra of Q bands in Figure 2a. Comparing the ratio of absorbances at the Soret and Q-bands, it can be seen that the relative intensity of Q-bands of the hybrid POR-F/TiO₂ film is much higher than that of pure organic solutions. In addition, a similar result is also obtained from the UV spectra of hybrid POR-P/TiO₂ films and pure POR-P solution, as shown in Figure 2c,d. Therefore, the light absorption in the visible range is greatly enhanced through hybridizing pure organic dyes with TiO₂ nanoparticles. In other words, the synergic effect between TiO₂ nanoparticles and organic molecules increases the light-harvesting efficiency (LHE). It has been noticed that the incident photon-to-electron conversion efficiency (IPCE), which is the ratio of the number of photons incident to the solar cell to the number of collected electrons, is usually in a strong positive correlation with LHE. Thus, the hybrid organic dye/TiO₂ nanostructures can be potentially used as a good light harvester to improve the IPCE of solar cells.

Their microstructures were investigated by extensive HRTEM examinations to clarify the enhanced light absorption for the hybrid nanostructures. Figure 3a shows a typical BF TEM image of the hybrid organic dye/TiO₂ nanoparticles. In Figure 3a, one can see two types of TiO₂ nanoparticles surrounded by organic dyes, one being nearly spherical and the other being elongated. To give a reliable prevalence distribution of different types, we recorded more than 100 nanoparticles and carried out a statistical analysis of the different types among the overall population. The volume fraction of TiO₂ nanoparticles with nearly spherical morphology (~73.3% of total nanoparticles) is higher than that of the nanoparticles with elongated morphology (~26.7% of total nanoparticles). Examinations of more than 100 nanoparticles show that the edge length of the particles ranges from 10 to 30 nm. Furthermore, it is interesting to find that the organic dyes are adsorbed only on part of but not all of the TiO₂ nanoparticles. Figure 3b is a typical HRTEM image of pure TiO₂ nanoparticles with nearly spherical morphology and a diameter of ~25 nm. From Figure 3b, one can see that the interplanar distance of nanoparticle is ~3.48 Å, corresponding to the lattice spacing of anatase TiO₂ {101} planes. It can be seen that the nanoparticle edge is very clean and the contrast of the amorphous region is homogeneous, which is identified to be the carbon film.

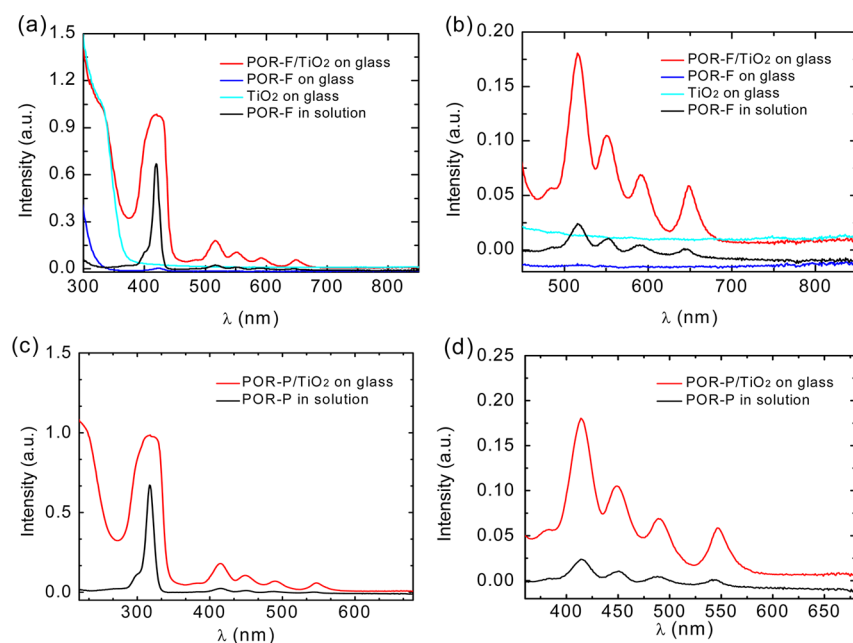


Figure 2. Normalized steady-state UV–vis absorption spectra (a) and the zoomed absorption Q-band spectra (b) of hybrid POR-F/TiO₂ and pure POR-F solution. Normalized steady-state UV–vis absorption spectra (c) and the zoomed Q-band spectra (d) of hybrid POR-P/TiO₂ and pure POR-P solution.

Figure 3c,d and Figure 3e,f present typical HRTEM images of hybrid POR-P/TiO₂ and POR-F/TiO₂ nanostructures, respectively. From these HRTEM images, it can be seen that the contrast of the amorphous regions is not homogeneous, which is distinguished by the dashed lines. The contrast of the regions close to the TiO₂ nanoparticles is dark, while the region a little far away from the nanoparticles is light. Compared with the pure carbon film, the attached POR-P or POR-F molecules onto the TiO₂ nanoparticles increase the sample thickness, which leads to the darker contrast of the region near the nanoparticles. Careful examinations of Figure 3c,d show that more POR-P molecules are attached on the {101} surfaces, while less POR-P molecules are adsorbed on the (102) and (110) surfaces of TiO₂ nanoparticles. From Figure 3e,f, it can be found that POR-F molecules have a priority to be adsorbed on (101) planes rather than (100) planes of TiO₂ nanoparticles. Therefore, both POR-P and POR-F molecules are preferentially adsorbed onto the {101} surfaces of anatase TiO₂ nanoparticles, which might be attributed to the enhanced light absorption.

For anatase TiO₂, {101} surfaces are the most thermally stable with a surface occupancy rate >90%,¹⁸ which can be naturally obtained without addition of HF or other morphology-directing agents during the fabrication process. Therefore, it is very advantageous for the organic dyes to be preferentially adsorbed onto the {101} facets of TiO₂ nanoparticles to form hybrid nanostructures.

DFT calculations were performed to investigate the adsorption behaviors of organic dyes onto anatase TiO₂ (101), (100), (110), and (102) surfaces to reveal the preferential attachment mechanism. From Figure 1c,d, it can be seen that the structures of both organic compounds are very complicated, which makes it very difficult to carry out the DFT calculations; however, careful examinations show that the ends of both organic molecules have similar functional groups, –PO(OH)₂ and –COOH, the latter of which is considered to act as the connection between POR-F molecule and anatase

TiO₂ surfaces.^{19–21} Therefore, a simplified and small molecule of HCOOH, as shown in Figure 4a, is adopted as a model to represent both organic molecules. All optimized geometrical structures were calculated using DMol³ Package in Materials Studio.²² The Perdew–Burke–Ernzerhof (PBE), one kind of generalized gradient approximation (GGA),²³ was used for the functional of exchange–correlation. The valence orbitals of the atoms were described by setting the double-numeric quality with polarization functions (DNP),²⁴ and the core electrons were substituted by DFT semicore pseudopotentials (DSPPs).²⁵ The configurations were considered to be completely stable until the energy change $<2.0 \times 10^{-5}$ Ha/atom, the residual force was <0.004 Ha/Å, and the maximum displacement was <0.005 Å.²⁶ To make sure that the calculation results were reliable, the full optimization of pure anatase TiO₂ structure was performed. The computed lattice parameters of the anatase TiO₂ crystal ($a = b = 3.776$ Å, $c = 9.486$ Å) are in good agreement with experimental measurements ($a = b = 3.785$ Å, $c = 9.514$ Å),²⁷ which further implied that our calculation method was reasonable.

The adsorption energy, E_{ads} , was calculated according to the following equation.

$$E_{\text{ads}} = E_{\text{HCOOH}} + E_{\text{surface}} - E_{\text{HCOOH/surface}}$$

where E_{ads} is the adsorption energy of HCOOH, $E_{\text{HCOOH/surface}}$ is the total energy of the HCOOH/surface system with one or more molecules adsorbed on surfaces, and E_{surface} is the total energy of clean anatase (101), (100), (110), or (102) surface slab. According to the previous equation, a positive value stands for an energetically favorable adsorption configuration. The more positive the adsorption energy, the more stable the adsorption configuration.

On the basis of the electrostatic interactions, several possible adsorption geometries of every surface were considered. Figure 4b–e shows the optimized configurations of HCOOH adsorbed on anatase TiO₂ (101), (110), (100), and (102) surfaces, respectively. In all adsorption configurations, both

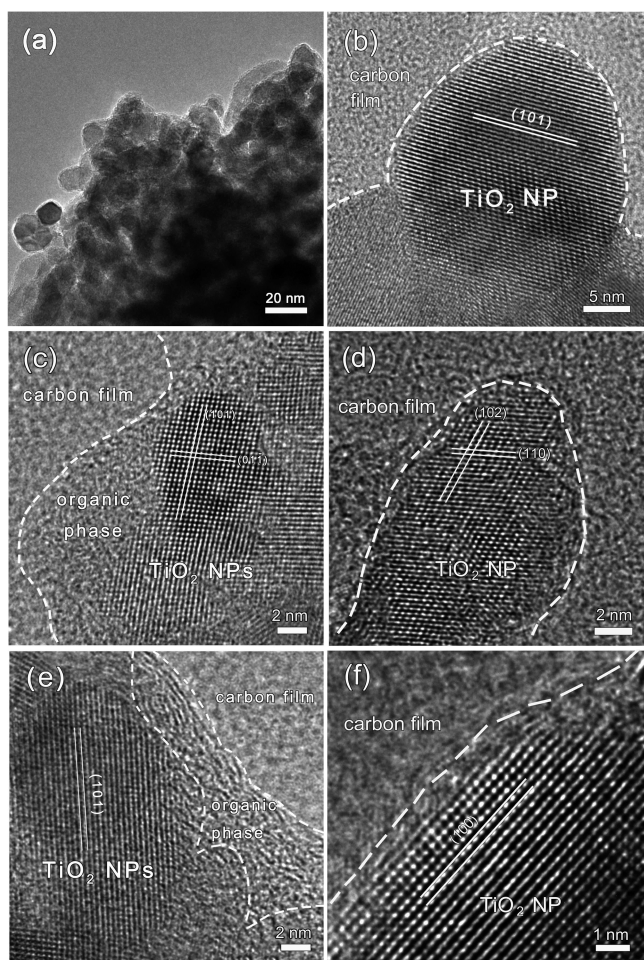


Figure 3. (a) BF TEM image of the hybrid organic/TiO₂ nanostructures; (b) HRTEM image of pure TiO₂ nanoparticles; (c,d) HRTEM images of the hybrid POR-P/TiO₂ nanostructures; and (e,f) HRTEM images of the hybrid POR-F/TiO₂ nanostructures.

structures of adsorbed HCOOH and anatase TiO₂ (101), (110), (100), and (102) surfaces have very little distortion with

a displacement of about 0.01 to 0.03 Å compared with the isolated HCOOH molecule and the clean surfaces. An important role in stabilizing these adsorption structures is played by the hydrogen bonds with the bond lengths ranging from 1.513 to 1.608 Å between the hydroxyl proton of HCOOH and the O atoms on the surfaces. Meanwhile, the Ti atoms on these surfaces are attacked through the carbonyl oxygen with a distance ranging from 2.125 to 2.232 Å. All of these energetic and structural properties indicate that the adsorption states of HCOOH on anatase TiO₂ surfaces belong to typical physisorption.

Table 1 summarizes the calculated adsorption properties of HCOOH on anatase TiO₂ (101), (110), (100), and (102)

Table 1. Properties of HCOOH Adsorbed on the Different Facets of Anatase TiO₂

facets	minimum periodicity (Å)	E_{ads} (eV)	q (e)
(101)	5.412	0.942	0.163
(110)	5.871	1.248	0.143
(100)	9.486	0.766	0.162
(102)	12.125	unstable	

surfaces. The calculated adsorption energies are 0.942, 1.248, and 0.766 eV for the configurations on anatase TiO₂ (101), (110), and (100) surfaces, respectively, while the adsorption energy for the configuration on TiO₂ (102) surface does not correspond to any local minimum. The computed adsorption energies imply that the most preferential adsorption surface is (110) surface and the second is (101) surface, which are consistent with the previous theoretical results that (110) surfaces are more reactive than (101) surfaces.^{28,29} The calculated preferential adsorption on (110) surfaces seems contradictory to the experimental results disclosed in the HRTEM images; however, it can be seen from Table 1 that the charge transfer of HCOOH molecule on anatase TiO₂ (110) surface (0.143e) is much lower than that of anatase (101) surface (0.163e). The lower charge transfer on the (110) surface is inconsistent with its higher adsorption energy, which is usually in a strong positive correlation in many cases.³⁰ This difference indicates that some other factors, such as the

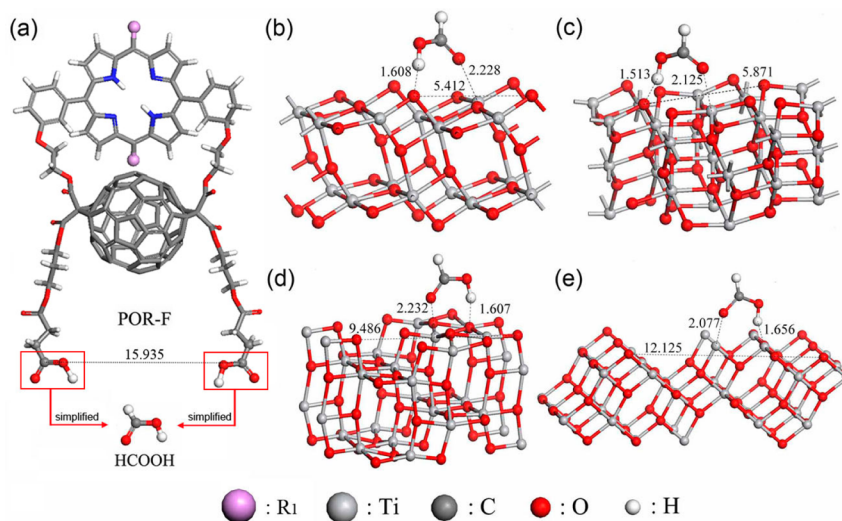


Figure 4. Optimized geometrical structures of POR-F (a) and HCOOH adsorbed on anatase TiO₂ (101) surface (b), (110) surface (c), (100) surface (d), and (102) surface (e).

geometrical match, contribute to the higher adsorption energy on the anatase TiO₂ (110) surface in addition to the electrostatic interaction. Actually, to correctly predict how a molecule is adsorbed on a metal oxide surface, not only the chemical state but also the local coordination of the adsorption sites should be considered as a result of the presence of secondary interactions.³¹ As can be seen from Figure 4c, the surface configuration has a deeper trough on the (110) surface than that on the (101) surface, which provides more chances for the HCOOH molecules to be adsorbed deep enough to generate a strong adsorption energy. In addition, in the adsorption configuration of HCOOH on TiO₂ (110) surfaces, two O atoms surround the adsorbed O atom, providing a synergic effect to enhance the stability and adsorption energy of the system, while similar structures cannot be found on (101) and (100) surfaces corresponding to the relatively low adsorption energy.

To give a more reasonable explanation, the geometrical configuration of real dye molecules has to be taken into account. POR-F molecule is much larger than HCOOH, and the advantageous geometrical match between the HCOOH molecule and TiO₂ (110) surfaces cannot be retained. Moreover, the periodicity of extended width on the surface can also be a factor influencing the adsorption stability. The distance between the two ends of the branches of POR-F molecular unit (15.935 Å), as shown in Figure 4a, is about three times the atomic arrangement periodicity of the TiO₂ (101) surface (5.412 Å × 3 = 16.236 Å), which indicates that the structure of POR-F molecule is more inclined to match with the TiO₂ (101) surfaces rather than (110) surfaces. Al-Saidi et al.³² reported a similar result that small differences in the binding energies of the repeated units could lead to strong preferences for chain binding to a particular surface, and they also demonstrated the adsorption differences for small molecule and polymeric molecule. Therefore, the preferential adsorption of organic dye molecules on TiO₂ (101) surfaces is reasonable.

CONCLUSIONS

The hybrid organic dye/TiO₂ nanoparticles are successfully fabricated by the self-assembly method. The preferential attachment of organic dyes onto TiO₂ {101} facets, observed by HRTEM, greatly contributes to the enhanced light absorption of the hybrid nanostructures. Such preferential attachment is further confirmed by DFT calculations, which is attributed to the strong electrostatic interaction and competitive geometrical configuration of (101) facets. The results may provide useful guidance for the controllable synthesis of hybrid nanostructures and for their applications in solar cells.

AUTHOR INFORMATION

Corresponding Author

*E-mail: yqwang@qdu.edu.cn. Tel: +86-532-83780318.

Notes

The authors declare no competing financial interest.

ACKNOWLEDGMENTS

We thank the financial support from the National Key Basic Research Development Program of China (grant no. 2012CB722705), the Natural Science Foundation for Outstanding Young Scientists in Shandong Province, China (grant no. JQ201002), and High-end Foreign Experts Recruitment Program (grants nos. GDW20143500163,

GDW20133400112). Y.W. acknowledges the financial support from the Top-notch Innovative Talent Program of Qingdao City (grant no. 13-CX-8) and the Taishan Scholar Program of Shandong Province, China. F.T. acknowledges the financial support from the National Natural Science Foundation of China (grant no. 20703027 and Shandong Excellent Young Scientist Research Award Fund (grant no. BS2011NJ004).

REFERENCES

- (1) Walter, M. G.; Warren, E. L.; McKone, J. R.; Boettcher, S. W.; Mi, Q. X.; Santori, E. A.; Lewis, N. S. Solar Water Splitting Cells. *Chem. Rev.* **2010**, *110*, 6446–6473.
- (2) Jin, X.; Sun, W. F.; Chen, Z. H.; Li, Y.; Li, P. J.; He, X. D.; Yuan, Y. B.; Zou, S. B.; Qin, Y. C.; Li, Q. H. Efficient Electron/Hole Transport in Inorganic/Organic Hybrid Solar Cells by Lithium Ion and Molybdenum Trioxide Codoping. *J. Power Sources* **2014**, *268*, 874–881.
- (3) Desai, U. V.; Xu, C. K.; Wu, J. M.; Gao, D. Hybrid TiO₂-SnO₂ Nanotube Arrays for Dye-Sensitized Solar Cells. *J. Phys. Chem. C* **2013**, *117*, 3232–3239.
- (4) Lira-Cantu, M.; Chafiq, A.; Faissat, J.; Gonzalez-Valls, I.; Yu, Y. H. Oxide/Polymer Interfaces for Hybrid and Organic Solar Cells: Anatase vs. Rutile TiO₂. *Sol. Energy Mater. Sol. Cells* **2011**, *95*, 1362–1374.
- (5) Abrusci, A.; Stranks, S. D.; Docampo, P.; Yip, H.; Jen, A. K. Y.; Snaith, H. J. High-Performance Perovskite-Polymer Hybrid Solar Cells via Electronic Coupling with Fullerene Monolayers. *Nano Lett.* **2013**, *13*, 3124–3128.
- (6) Fujishima, A.; Honda, K. TiO₂ Photoelectrochemistry and Photocatalysis. *Nature* **1972**, *238*, 37–38.
- (7) Hadjiivanov, K. I.; Klissurski, D. G. Surface Chemistry of Titania (Anatase) and Titania-Supported Catalysts. *Chem. Soc. Rev.* **1996**, *25*, 61–69.
- (8) Linsebigler, A. L.; Lu, G. Q.; Yates, J. T. Photocatalysis on TiO₂ Surfaces: Principles, Mechanisms, and Selected Results. *Chem. Rev.* **1995**, *95*, 735–758.
- (9) Chen, X. B.; Mao, S. S. Titanium Dioxide Nanomaterials: Synthesis, Properties, Modifications, and Applications. *Chem. Rev.* **2007**, *107*, 2891–2959.
- (10) Steim, R.; Kogler, F. R.; Brabec, C. J. Interface Materials for Organic Solar Cells. *J. Mater. Chem.* **2010**, *20*, 2499–2512.
- (11) Steim, R.; Choulis, S. A.; Schilinsky, P.; Brabec, C. J. Interface Modification for Highly Efficient Organic Photovoltaics. *Appl. Phys. Lett.* **2008**, *92*, 093303.
- (12) Lira-Cantu, M.; Norrman, K.; Andreasen, J. W.; Krebs, F. C. Oxygen Release and Exchange in Niobium Oxide MEHPPV Hybrid Solar Cells. *Chem. Mater.* **2006**, *18*, 5684–5690.
- (13) Gonzalez-Valls, I.; Lira-Cantu, M. Dye Sensitized Solar Cells Based on Vertically Aligned ZnO Nanorods: Effect of UV Light on Power Conversion Efficiency and Lifetime. *Energy Environ. Sci.* **2010**, *3*, 789–795.
- (14) Mihailetchi, V. D.; Blom, P. W. M.; Hummelen, J. C.; Rispen, M. T. Cathode Dependence of the Open-circuit Voltage of Polymer: Fullerene Bulk Heterojunction Solar Cells. *J. Appl. Phys.* **2003**, *94*, 6849–6854.
- (15) Rand, B. P.; Burk, D. P.; Forrest, S. R. Offset Energies at Organic Semiconductor Heterojunctions and their Influence on the Open-Circuit Voltage of Thin-film Solar Cells. *Phys. Rev. B* **2007**, *75*, 115327.
- (16) Lo, M. F.; Ng, T. W.; Liu, T. Z.; Roy, V. A. L.; Lai, S. L.; Fung, M. K.; Lee, C. S.; Lee, S. T. Limits of Open Circuit Voltage in Organic Photovoltaic Devices. *Appl. Phys. Lett.* **2010**, *96*, 113303.
- (17) Li, C. Y.; Wang, J. B.; Wang, Y. Q. Microstructure and Photocatalytic Activity of Titanium Dioxide Nanoparticles. *Chin. Phys. B* **2012**, *21*, 098102.
- (18) Lazzeri, M.; Vittadini, A.; Selloni, A. Structure and Energetics of Stoichiometric TiO₂ Anatase Surfaces. *Phys. Rev. B* **2001**, *63*, 155409.

(19) Wang, H. G.; Zhou, D. M.; Wu, Z. Z.; Wan, J. M.; Zheng, X. M.; Yu, L. H.; Phillips, D. L. The Visible Light Degradation Activity and the Photocatalytic Mechanism of Tetra(4-Carboxyphenyl) Porphyrin Sensitized TiO₂. *Mater. Res. Bull.* **2014**, *57*, 311–319.

(20) Mathew, S.; Iijima, H.; Toude, Y.; Umeyama, T.; Matano, Y.; Ito, S.; Tkachenko, N. V.; Lemmetyinen, H.; Imahori, H. Optical, Electrochemical, and Photovoltaic Effects of an Electron-Withdrawing Tetrafluorophenylene Bridge in a Push-Pull Porphyrin Sensitizer Used for Dye-Sensitized Solar Cells. *J. Phys. Chem. C* **2011**, *115*, 14415–14424.

(21) Subramanian, V.; Wolf, E. E.; Kamat, P. V. Catalysis with TiO₂/gold Nanocomposites. Effect of Metal Particle Size on the Fermi Level Equilibration. *J. Am. Chem. Soc.* **2004**, *126*, 4943–4950.

(22) Delley, B. From Molecules to Solids with the DMol³ Approach. *J. Chem. Phys.* **2000**, *113*, 7756–7764.

(23) Perdew, J. P.; Burke, K.; Ernzerhof, M. Generalized Gradient Approximation Made Simple. *Phys. Rev. Lett.* **1996**, *77*, 3865–3868.

(24) Inada, Y.; Orita, H. Efficiency of Numerical Basis Sets for Predicting the Binding Energies of Hydrogen Bonded Complexes: Evidence of Small Basis Set Superposition Error Compared to Gaussian Basis Sets. *J. Comput. Chem.* **2008**, *29*, 225–232.

(25) Delley, B. Hardness Conserving Semilocal Pseudopotentials. *Phys. Rev. B* **2002**, *66*, 155125.

(26) Tian, F. H.; Wang, X. B.; Zhao, W. W.; Zhao, L. H.; Chu, T. S.; Yu, S. Q. Adsorption of 2-Propanol on Anatase TiO₂ (101) and (001) Surfaces: a Density Functional Theory Study. *Surf. Sci.* **2013**, *616*, 76–84.

(27) Cromer, D. T.; Herringt, K. The Structures of Anatase and Rutile. *J. Am. Chem. Soc.* **1955**, *77*, 4708–4709.

(28) Sanches, F. F.; Mallia, G.; Liborio, L.; Diebold, U.; Harrison, N. M. Hybrid Exchange Density Functional Study of Vicinal Anatase TiO₂ Surfaces. *Phys. Rev. B* **2014**, *89*, 245309.

(29) Lazzeri, M.; Vittadini, A.; Selloni, A. Structure and Energetics of Stoichiometric TiO₂ Anatase Surfaces. *Phys. Rev. B* **2002**, *65*, 119901.

(30) Zhao, W. W.; Tian, F. H.; Wang, X. B.; Zhao, L. H.; Wang, Y.; Fu, A. P.; Yuan, S. P.; Chu, T. S.; Xia, L. H.; Yu, J. C.; Duan, Y. B. Removal of Nitric Oxide by the Highly Reactive Anatase TiO₂ (001) Surface: A Density Functional Theory Study. *J. Colloid Interface Sci.* **2014**, *430*, 18–23.

(31) Vittadini, A.; Selloni, A.; Rotzinger, F. P.; Grätzel, M. Formic Acid Adsorption on Dry and Hydrated TiO₂ Anatase (101) Surfaces by DFT Calculations. *J. Phys. Chem. B* **2000**, *104*, 1300–1306.

(32) Al-Saidi, W. A.; Feng, H. J.; Fichthorn, K. A. Adsorption of Polyvinylpyrrolidone on Ag Surfaces: Insight into a Structure-directing Agent. *Nano Lett.* **2012**, *12*, 997–1001.